3 Methods of Characterization of 3D-Printed Objects

Yuanyuan Chen

3.1 INTRODUCTION

The popularity of 3D printers has increased in the past decade, partially attributed to the expiration of significant patents and the availability of cost-effective equipment. The utilisation of 3D printing technology offers numerous benefits, including cost efficiency, expedited prototyping, minimised waste production, the ability to create lightweight structures, and decreased energy consumption, among others. According to a recent study, the global market for 3D printing products and services reached an estimated value of approximately 12.6 billion USD in the year 2020. Projections indicate that this market is poised to have a compound annual growth rate of 17% throughout the period spanning 2020 to 2023 [1]. The utilisation of 3D printing technology has been observed in various domains, including but not limited to medical devices and the automobile industry, electronics sector, construction field, and aerospace sector. This chapter will elucidate the primary techniques employed for characterising three-dimensional printed objects.

3.2 DIMENSIONAL ACCURACY TESTING

The assessment of dimensional accuracy holds significant importance in the realm of 3D-printed products. The primary approach for evaluating the precision of 3D-printed things involves comparing them with their corresponding digital models.

Callipers are widely utilised instruments for assessing dimensional correctness. The primary dimensions include height, width, length, diameter, and other relevant measurements. The assessment of linear dimensional correctness in 3D-printed objects involves the measurement of their dimensions along the X-direction, Y-direction, and Z-direction. Dimensional errors can be quantified by determining the disparity between the physical dimension and the corresponding dimension in the digital model. In their study, Carew et al. employed three different 3D printing technologies, fused deposition modelling (FDM), selective laser sintering (SLS), and stereolithography (SLA), to fabricate 3D-printed replicas of skeletal elements obtained from computed tomography (CT) scans. These replicas were utilised for the purpose of reconstructing forensic anthropology evidence. To assess the accuracy of the 3D-printed replicas, the dimensions of both the physical replicas and virtual 3D models were compared using callipers. The study revealed that every

DOI: 10.1201/9781003415985-3

printer generated replicas with mean differences falling within the range of ±1.2 mm. Furthermore, the printer utilising the SLS technique demonstrated the highest level of accuracy and produced prints that closely resembled the original CT scan in terms of aesthetics.

Nevertheless, a significant number of 3D-printed items possess intricate geometries, such as personalised medical apparatus, hence imposing limitations on the precision achievable through calliper measurements. The dimensional accuracy verification of complicated 3D-printed objects is frequently conducted using a coordinate measuring machine (CMM) (Figure 3.1a). The process involves the utilisation of a probe to detect discrete points on the surface of physical objects, hence enabling the measurement of their geometry.

In their study, Kacmarcik et al. conducted an analysis of the accuracy performance of two FDM 3D printers, the Ultimaker 2+ and ZEN3D. The samples were designed using SolidWorks, computer-aided design (CAD) software, incorporating various geometric elements such as cylinders, circles, cuboids, and squares. Subsequently, two FDM printers were employed to fabricate the designed samples. To assess the accuracy of the 3D-printed items, their dimensions and tolerances were measured using CMM scans. Finally, the variations in the dimensional parameters of the printed samples were determined. According to the findings, the Ultimaker 2+ printer exhibited superior dimensional accuracy in comparison to the ZEN3D printer [2].

Sandhu et al. conducted a study in which they utilised an FDM 3D printer to fabricate a drilling bit using acrylonitrile-butadiene-styrene (ABS) material. The researchers employed a CMM to assess any variations in the width and depth of the cut or groove generated by the ABS drilling bit. The findings of their investigation indicated that the 3D-printed drilling bit exhibited the ability to effectively machine soft materials while maintaining precise dimensional and topographic characteristics [3].

In order to enhance the precision of CMM, the integration of a micro tactile probe might be considered. This integration is particularly useful for accurately measuring intricate geometric features within the millimetre to micrometre scale, as depicted in Figure 3.1b [4]. The application of laser beams for ultra-high-precision measurement on the CMM was described, resulting in a measurement accuracy of ±6 μm [5].

Image analysis is another frequently employed method for evaluating the dimensional precision of 3D-printed items. This approach entails capturing visual representations of the 3D-printed artefact and juxtaposing them with the design model, subsequently computing the geometric disparities between the two.

Lin conducted research on the development of several resins specifically designed for UV digital light 3D printing. Additionally, Lin assessed the precision and fidelity of the printing materials by conducting a comparative analysis between the physical 3D-printed models and their corresponding digital models. The master digital model of a typodont molar was obtained by scanning it using an intraoral scanner. Subsequently, the digital molar model was replicated by printing it using formulated resins. The printed molars were then rescanned and compared to the master digital model in order to assess any deviations that occurred during the printing process. According to the paper, a 3D printing resin was developed using a composition consisting of 80% ethoxylated bisphenol A-dimethacrylate, 10% urethane

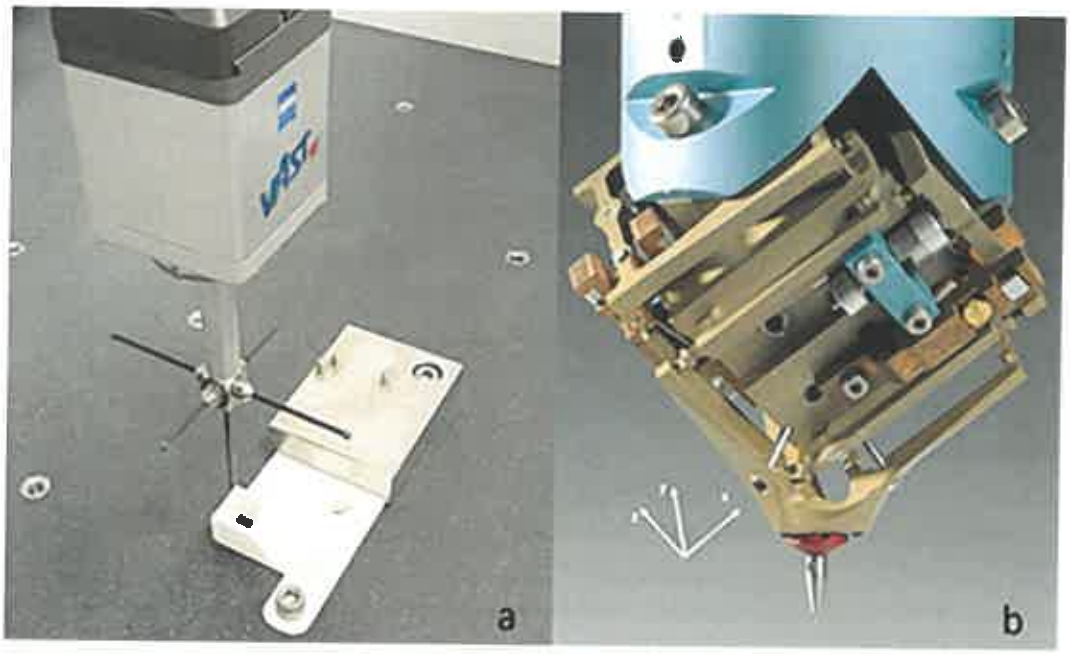

FIGURE 3.1 a) CMM for measuring 3D-printed objects. Adapted from [2]. Copyright the authors, some rights reserved; exclusive licensee IOP Publishing. Distributed under a Creative Commons Attribution License 4.0 (CC BY). b) Tactile microprobe for CMM. Adapted from [4]. Copyright the authors, some rights reserved; exclusive licensee MDPI. Distributed under a Creative Commons Attribution License 4.0 (CC BY).

dimethacrylate, and 10% triethylene glycol dimethacrylate. The resin was found to exhibit great precision and is deemed suitable for potential clinical applications in the future [6].

In their study, Fang et al. established an online methodology for image processing by incorporating geometric disparities into a closed-loop control system. The feedback mechanisms pertaining to the geometric disparities serve to rectify any flaws in the 3D printing procedure, hence facilitating the real-time detection and monitoring of errors [7]. In order to enhance the validity of the data collected, Straub devised multi-camera system and image processing software for the evaluation of access printing progress [8].

3.3 MORPHOLOGY AND SURFACE FINISH EVALUATION

The initial stage in examining the morphology and surface texture of 3D-printed objects involves doing an optical research. Certain faults can be readily detected, including over- and under-fill, loss of continuity, uneven layer marks, and irregular layers, among others.

An optical microscope, commonly referred to as a light microscope, employs optical principles to generate magnified images of minute sections of 3D-printed objects in order to detect any faults. In their study, Gkartzou et al. employed an optical microscope to examine the morphology of individual fibres that were extruded under various printing speeds, printing temperatures, and fibre widths [9].

The utilisation of a confocal microscope is frequently employed in the examination of surface roughness in 3D-printed objects. This instrument enables the optical segmentation of the surface, which is subsequently transformed into digital images and a topographic map through computational processing. By employing an algorithm, the computer is able to analyse the topographic map and derive a roughness parameter that effectively characterises the texture of the surface [10]. In their study, Polzin et al. employed a confocal microscope to examine 3D-printed items made from poly(methyl methacrylate) (PMMA). Their findings indicated that the introduction of wax infiltration led to a reduction in surface roughness of these things by as much as 50% [11].

The utilisation of an atomic force microscope (AFM) presents itself as a valuable instrument for the examination of surface roughness in the context of 3D-printed artefacts. The system functions based on the concept of surface sensing, employing a highly precise tip located on a micromachined silicon probe. The tip is affixed to a diminutive cantilever structure, so that when the tip comes into contact with the surface of the test material, the cantilever undergoes deflection, thereby providing an indication of the surface condition of the test material. In their study, Gorji et al. employed AFM as a means to investigate the surface roughness characteristics of stainless steel 316L powders, specifically in the context of powder bed fusion 3D printing [12].

The presence of air voids and pores within 3D-printed items is a widely seen phenomenon. The application of X-ray computed tomography (XCT) has been employed for the assessment of pore distribution and pore size within 3D-printed plastic and concrete structures. XCT employs a chromatic X-ray cone beam as a non-contact radiation medium in order to reveal the 3-dimensional geometric characteristics using a non-destructive methodology. In their study, Wang et al. employed XCT as a means to quantify the presence of air voids within FDM 3D-printed items. The dispersion and the size of the voids can be measured directly on the XCT images [13]. The void content or porosity of a sample can be measured by comparing the weight of wet samples and dried samples with Eq. (1):

$$Porosity = \frac{W_{wet} - W_{dry}}{W_{wet}} \times 100\% \qquad \text{Eq. (1)}$$

Mercury intrusion porosimetry (MIP) is a commonly employed technique for the characterisation of 3D-printed concrete materials. This method entails the application of pressure to introduce mercury into the pores of the sample, followed by the measurement of the volume of mercury utilised. The selection of mercury for the porosity study was based on its non-wetting characteristic, ensuring that it does not get absorbed by the test samples. Additionally, the need for external pressure to fill the spaces contributes to the high accuracy of porosity measurements [14]. The quantification of air voids present in 3D-printed concrete, mortar, and grout objects can be accomplished by adhering to the DIN EN 480–4 standard. This involves assessing the quantity of mixing water within the concrete, which can be segregated by analysing samples of fresh concrete both with and without admixtures.

Electron microscopy includes various techniques, including scanning electron microscopy (SEM), transmission electron microscopy (TEM), and field emission scanning electron microscopy (FESEM), which employ an accelerated electron beam rather than relying on light waves as in optical microscopy. The flow of electrons has both particle-like and wave-like properties, resulting in significant amplification and enhanced clarity. The utilisation of electron microscopy is frequently employed for the examination of the morphological characteristics of objects produced using three-dimensional printing techniques. Liu et al. utilised SEM to observe the voids between each layer of the items 3D printed via fused granule fabrication [15]. Nguyen et al. conducted a study wherein they generated a composite material for FDM 3D printing. They employed SEM to examine the flow direction or orientation of cellulose fibres within the polymer matrix during the 3D printing procedure [16].

3.4 MECHANICAL TESTING

Currently, there is a lack of universally accepted test protocols for the purpose of mechanically characterising things produced by 3D printing technology. Consequently, the mechanical properties of 3D-printed things have been evaluated by typical testing for objects produced using conventional methods. These tests include tension, compression, bending, fatigue loading, impact loading, and creep [17]. Table 3.1 presents the mechanical test standards utilised by the American Society for Testing Materials (ASTM) and the International Organisation for Standardisation (ISO) in the evaluation of 3D-printed products.

The mechanical parameters that are commonly evaluated for 3D-printed objects include Young's modulus, yield strength, ultimate strength, shear modulus, storage and loss modulus, elasticity, and elongation at break. Various mechanical properties can be ascertained through the utilisation of diverse testing methodologies. For example, the stress–strain relationship and Young's modulus of a material can be assessed through a tensile test. The shear modulus of a material can be determined by conducting either a static torsion test or a dynamic oscillatory rheometer. The hardness of a material can be evaluated using various hardness tests, such as the Brinell, Rockwell, and Vickers hardness tests. The toughness of a material can be measured through the Charpy test. The deformation behaviour of a material can be analysed using creep and fatigue tests. Metallographic analysis is commonly employed for the examination of metal 3D printing processes.

Ideally, it is envisioned that the mechanical qualities of 3D-printed things will closely resemble those of objects produced using traditional manufacturing processes. Nevertheless, the utilisation of the layer-to-layer production technique in 3D printing gives rise to interfacial weakness, resulting in anisotropy and heterogeneous mechanical characteristics. In their study, Ahn et al. conducted a comparison of the mechanical qualities between items produced using FDM printing and injection moulding. Their findings indicated that the FDM-printed objects exhibited around 70% and 85% of the tensile and compressive strength, respectively, when compared to the injection moulded products [18].

TABLE 3.1
Commonly Used ASTM and ISO Standards for Mechanical Property Characterisation

Standards	Type of Mechanical Testing	Test Material
ASTM D638	Tensile test	Plastics
ASTM D412	Tensile test	Vulcanised rubber and thermoplastic elastomers
ASTM D882	Tensile test	Thin plastic sheeting
ASTM D3039	Tensile test	Polymer composites
ISO 527	Tensile test	Plastics
ISO 37	Tensile test	Thermoplastic and vulcanised rubbers
ASTM D790	Flexural test	Plastics and electrical insulating materials
ISO 178	Flexural test	Rigid and semi-rigid plastics
ASTM D1938	Tear propagation resistance	Plastic film or sheeting
ISO 34	Tear test	Rubber, vulcanised or thermoplastics
ASTM D695–02a	Compression test	Rigid plastics
ASTM C109	Compressive test	Concrete
ISO 604	Compressive test	Rigid plastics
ASTM C348	Flexural test	Concrete
ASTM D3518	In-plane shear test	Polymer composites reinforced by fibres
ASTM D256	Izod impact test	Notched plastic
ASTM D6110	Charpy impact test	Notched plastic
ISO 180:2000	Izod impact test	Notched plastic
ISO 179–1:2010	Charpy impact test	Notched plastic
ISO 179–2:1997	Charpy impact test	Notched plastic
ASTM E384	Microindentation hardness test	Wide range of materials
ASTM D2240	Shore durometer hardness test	Elastomers
ASTM D785	Rockwell hardness test	Plastics
ISO 2039–1	Hardness test—ball indentation method	Plastics
ISO 2039–2:1987	Rockwell hardness test	Plastics
ASTM D2990	Tensile, compressive, flexural creep, and creep rupture	Plastics
ISO 899–1:2003C	Creep behaviour	Plastics
ISO 899–2:2003	Flexural creep behaviour by three-point loading	Plastics
ASTM D7791	Fatigue	Plastics
ASTM D3479	Fatigue	Polymer composites
ASTM D7774	Fatigue test under bending	Plastics
ISO 13003	Fatigue test	Fibre-reinforced plastics

The mechanical characteristics of three-dimensional printed items can be influenced by the materials utilised in the process of three-dimensional printing. Various types of reinforced 3D printing materials have been developed to enhance the mechanical properties of 3D-printed objects. These include short fibre-reinforced 3D printing material [19], long fibre-reinforced 3D printing material [20], continuous fibre-reinforced 3D printing material [21], and polymer composites [22].

The mechanical qualities of 3D-printed items have been seen to be influenced by the employed printing processes. The study conducted by Khosravani et al. examined the impact of raster orientations, namely the angle of the printing direction in relation to the loading direction, on the mechanical properties of 3D-printed things. The findings of the study indicated that as the raster direction increased, there was a corresponding drop in the strength of the 3D-printed products. According to the referenced study [23], the samples oriented at 0° exhibited the maximum level of strength, whilst the samples oriented at 90° demonstrated the lowest strength values. To clarify, optimal tensile properties are achieved when filaments are aligned longitudinally and parallel to the direction of loading, while the least favourable tensile properties are observed when samples are loaded along the build direction. This can be attributed to the inadequate bonding between layers [17].

In their study, Rankouhi et al. investigated the influence of layer thickness on the mechanical properties of 3D-printed objects. Their findings indicated that the specimens printed with a layer thickness of 0.2 mm demonstrated superior elastic modulus and ultimate strength when compared to those printed with a layer thickness of 0.4 mm. This disparity in mechanical properties can be attributed to the significantly reduced presence of air gaps between each bead or strand in the samples printed with a layer thickness of 0.2 mm, as opposed to those printed with a layer thickness of 0.4 mm [24].

Various 3D printing procedures yield distinct mechanical characteristics in the produced 3D-printed artefacts. The mechanical anisotropy of FDM is estimated to be roughly 50%, making it the highest among all available methods. The mechanical anisotropy of SLA is seen to be rather low, measuring at roughly 1%. Various parameters have been identified as potential influencers on the mechanical properties of SLA-printed items. These factors include curing wavelengths, annealing temperatures, resolution, and layer thickness, among others. Form Labs, a prominent producer in the field of SLA, recently released a white paper that investigates the influence of curing parameters on the mechanical characteristics of SLA-printed items. According to their findings, specimens exposed to a wavelength of 405 nm and subjected to a curing temperature of 60°C exhibited the most notable tensile strength and modulus [25]. The mechanical anisotropy of SLS is relatively low, estimated to be under 10%. Various parameters, such as energy density, laser power, scan spacing, and laser beam speed, have the potential to influence the mechanical properties of items manufactured using SLS technology.

3.5 CHEMICAL PROPERTY TESTING

The assessment of the chemical composition of the 3D-printed object typically involves examining the impact of 3D printing techniques and the ageing process on

the objects, as well as exploring advancements in the development of new materials for 3D printing.

The Fourier transform infrared spectroscopy (FTIR) technique is employed to get an infrared spectrum that includes the absorption, emission, and photoconductivity characteristics of the substance under investigation. The characterisation of the chemical properties of 3D printing material is a widely employed practice. The detection of heat breakdown in thermoplastics during FDM 3D printing has been reported. The rise in absorption peaks for alkenes and aromatic chemicals can be attributed to heat deterioration in the context of ABS. The vibrational frequencies associated with alkenes and aromatic compounds are observed at wavenumbers of 3074, 1630, 910, 3033, 1496, and 698 cm^{-1} [26]. Polylactic acid (PLA) exhibits distinctive peaks at 1207 cm^{-1}, which can be attributed to the vibration of the alkyl-ketone chain, and at 920 cm^{-1}, which corresponds to the flexural vibration of the C-H bond. These peaks serve as indicators of the crystalline structure of PLA. However, the presence or absence of these peaks is influenced by the processing conditions. For instance, when fast cooling is employed during injection moulding, these peaks may vanish. Conversely, when a prolonged crystallisation process is carried out during annealing, these peaks may exhibit higher absorbance [27].

Raman spectroscopy is commonly employed for the purpose of characterising the structural properties of the material under investigation. This technique is based on the phenomenon of Raman scattering, wherein photons interact with molecular vibrations, so yielding a distinctive structural fingerprint of the molecules being analysed. The authors Roman et al. formulated inks containing lignin and graphene oxide for the purpose of 3D printing. To verify the presence of pyrolyzed carbon materials, Raman spectroscopy was employed, which revealed the typical bands at around 1350, 1580, and 2700 cm^{-1} [28]. Raman spectroscopy is frequently employed for the purpose of ascertaining the amorphous and crystalline characteristics of the substance under investigation. Trenfield et al. employed SLS 3D printing to fabricate tables containing hydroxypropyl cellulose. The researchers then utilised Raman spectroscopy as a means to quantitatively assess the amorphous composition of the 3D-printed pharmaceutical product [29].

The technique of nuclear magnetic resonance (NMR) utilises a robust and unchanging magnetic field to investigate the chemical composition of the specimen under examination. Kim et al. conducted a study in which they developed a bioink for digital light 3D printing using glycidyl methacrylate modified silk fibroin. To analyse the chemical properties of the bioink, proton NMR (H-NMR) spectroscopy was employed. The researchers measured the characteristic resonance of the methacrylate vinyl group ($\delta = 6.2–6$ and 5.8–5.6 ppm) and the methyl group of glycidyl methacrylate ($\delta = 1.8$ ppm). Additionally, they observed a decrease in the signal intensity of the lysine methylene group at $\delta = 2.9$ ppm, indicating a modification of the lysine residues present in the silk fibre [30]. Desai and Jagtap conducted a study in which they formulated a fibre reinforced resorcinol epoxy acrylate for use in SLA 3D printing. To assess the purity of the composite and confirm the occurrence of the chemical reaction, they employed carbon 13 nuclear resonance spectroscopy (13C-NMR). The analysis revealed specific resonation peaks at δ 132 ppm (C1) and δ 128 ppm (C2), which are indicative of the presence of acryloyl double bonds. Additionally, an

absorbance at δ 167.5 ppm (C3) was observed, corresponding to the carbonyl carbon of the ester component. The presence of absorbance peaks at δ 68.5 ppm (C6) and δ 160 ppm (C7) can be attributed to the oxygen connection with carbon, which signifies the production of the ether group. This observation provides evidence for the excellent purity of the composite, as it suggests the absence or minimum presence of any by-products [31].

X-ray diffraction (XRD) is a technique that utilises a beam of incident X-rays to interact with the crystalline structures of materials, resulting in the diffraction of X-rays in certain directions. By quantifying the intensity of the diffracted X-ray beams, it becomes possible to assess the crystallinity of the materials. XRD is commonly employed in the field of 3D printing material development to ascertain the level of crystallinity and the crystal structure of the materials. For example, researchers have successfully generated composite filaments for FDM 3D printing by combining PLA with lignin. These PLA/lignin composite filaments have demonstrated notable antibacterial and antioxidant capabilities, making them promising candidates for many healthcare applications [32]. PLA exhibits a wide peak within the range of 10° to 25° at 2θ degrees, which is attributed to the semicrystalline characteristics of PLA. The presence of peaks at 2θ = 32° and 34.5° in the PLA/lignin composites suggests that the PLA experienced further crystallisation, which can be attributed to the nucleating properties of lignin (Figure 3.2) [33].

X-ray photoelectron spectroscopy (XPS) is a quantitative spectroscopic technique that operates on the principles of the photoelectric effect, specifically for surface analysis. When subjected to x-ray irradiation, atoms on the near-surface of a material undergo the ejection of photoelectrons. The measurement of the kinetic energy of a

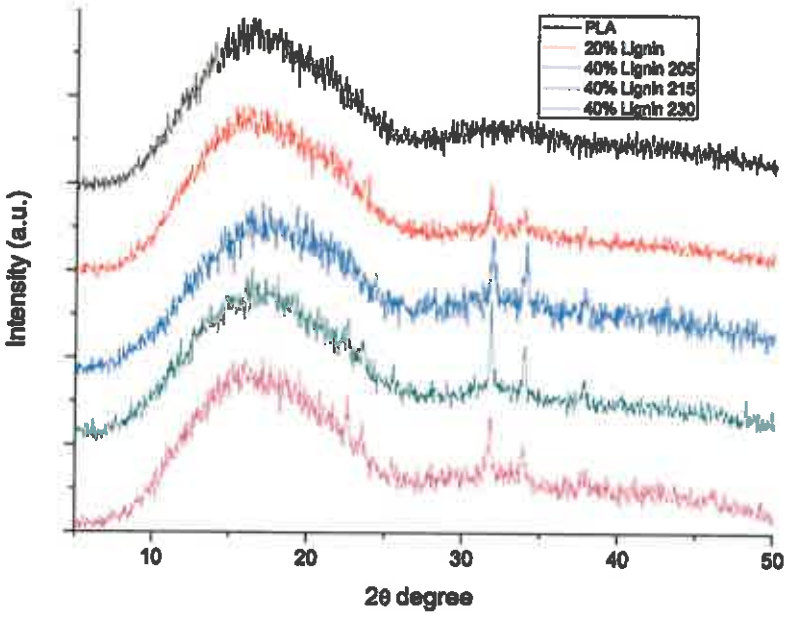

FIGURE 3.2 XRD patterns of PLA/lignin composites. Adapted from [33]. Copyright the authors, some rights reserved; exclusive licensee MDPI. Distributed under a Creative Commons Attribution License 4.0 (CC BY).

photoelectron that has been emitted can be conducted. XPS is frequently employed as a technique for quantifying the elemental composition in the context of material development for 3D printing. The researchers Hu et al. conducted a study in which they utilised a laser 3D printing technique to create objects by combining graphene and aluminium powder. To analyse the composition of the printed items, they employed XPS to quantify the presence of aluminium (Al), oxygen (O), and carbon (C) components on the surface [34].

Energy dispersive X-ray spectroscopy (EDX or EDS) is a widely employed analytical technique utilised for the purpose of elemental analysis or chemical characterisation of a given material. The X-ray beam engages in an interaction with the atoms present in the sample, resulting in the displacement of an electron from its shell, so creating a vacancy. Subsequently, an electron from a higher energy level fills this vacancy, leading to the release of energy. This emitted energy is then measured, and the energy levels of the resulting X-rays are used to establish a correlation with specific elements. In their study, Wang et al. successfully fabricated a magnetic covalent organic framework (COF) and bovine serum albumin (BSA) functionalised 3D-printed electrochemical biosensor. To validate the composition of the created material, the authors employed EDX analysis, which confirmed the presence of carbon (C), oxygen (O), nitrogen (N), sulphur (S), and iron (Fe) components [35].

Gel permeation chromatography (GPC) is a valuable analytical technique employed for the detection of chemical degradation through the quantification of alterations in molar mass. One example of a technique that employs the extrusion process is FDM 3D printing. This method requires the application of heat and shear force. The application of heat and stress to 3D-printed materials can result in a degree of deterioration and a reduction in molar mass. GPC has the capability to determine the molecular weight of materials before and after the 3D printing process. This enables the acquisition of conclusive data on material degradation, which is crucial for ensuring the quality of both the product and the manufacturing process. Furthermore, gas chromatography can be utilised to quantify the decrease in molar mass that occurs during the ageing process. This reduction is attributed to the degradation of chemical bonds resulting from factors such as fatigue, hydrolysis, oxidation, and exposure to UV radiation. Hence, GPC proves a valuable instrument for ascertaining the longevity of 3D-printed items and establishing appropriate storage parameters.

The assessment of particle emission in the atmosphere during 3D printing procedures has been conducted using a particle counter, scanning mobility particle sizer, and aerosol mass spectrometer. Research has indicated that the process of 3D printing results in the release of ultrafine particles. Among the commonly used materials, ABS emits a higher quantity of particles compared to PLA, primarily due to the elevated temperature required for printing. Furthermore, investigations utilising in vitro cellular assays have demonstrated the toxic nature of the particles emitted during the 3D printing process. Consequently, it is advisable to carry out 3D printing activities in well-ventilated environments, as recommended by previous studies [36].

3.6 THERMAL PROPERTY TESTING

Thermal analysis plays a crucial role in the context of hot melt extrusion-based 3D printing technology, namely in the case of FDM. The determination of the printing temperature and bed temperature during the 3D printing process is contingent upon the thermal parameters of the 3D printing material, including viscosity, glass transition temperature, melting temperature, and degradation temperature. Thermal analysis serves as a valuable characterisation tool in the development of innovative 3D printing materials, such as composites.

The printability or melt flow characteristic plays a crucial role in the FDM 3D printing process. If the printing qualities are not optimal, it becomes impossible to fabricate the object according to its intended design. The printability of a 3D printing material can be evaluated using a rheometer, a device that measures the viscosity of a material when subjected to external forces or stresses at elevated temperatures. An optimal printable substance should possess favourable shear-thinning properties to facilitate the process of melt extrusion. It is also crucial for the material to exhibit a very high zero-shear viscosity in order to provide the desired dimensional stability of the extruded melt subsequent to its discharge from the nozzle onto the printing bed. Nguyen et al. conducted a study to examine the printability of acrylonitrile-butadiene-styrene and high-impact polystyrene (HIPS) materials. Their findings on the optimal printing region are shown in Figure 3.3 [16].

Differential scanning calorimetry (DSC) is a widely employed technique in thermal analysis that enables the observation of material behaviour in response to controlled temperature variations, specifically with respect to heat flow rates. The provided data include the glass transition temperature, melting temperature, and crystallinity characteristics of a certain material. In their study, Damadzadeh et al. investigated the

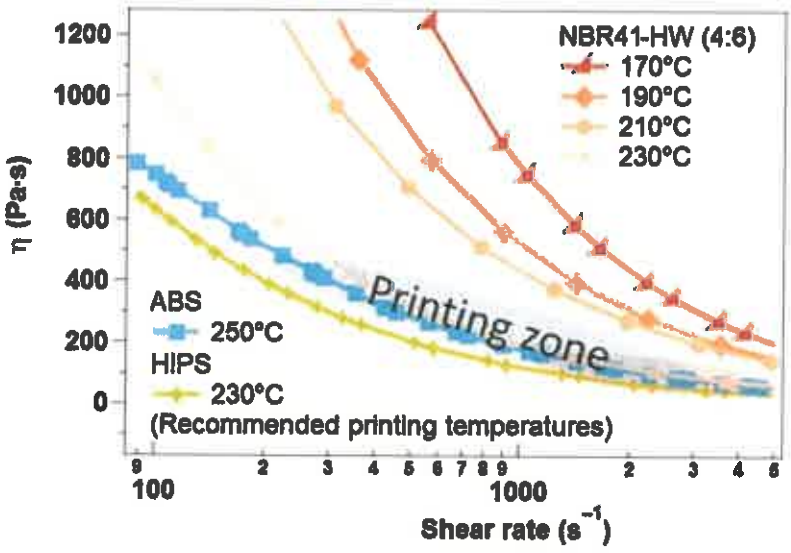

FIGURE 3.3 Viscosity of ABS, HIPS measured by rheology. Adapted from [16]. Copyright the authors, some rights reserved; exclusive licensee AAAS. Distributed under a Creative Commons Attribution License 4.0 (CC BY).

development of ceramic filler–reinforced composites using poly(lactic-co-glycolic acid (PLGA) and poly-L-lactic acid (PLLA) polymers for potential medical applications. The researchers observed that the incorporation of hydroxyapatite led to a reduction in the melting temperature of PLGA, as evidenced by the DSC curves. However, no significant impact on the melting temperature of PLLA was seen [37]. Composite filaments consisting of PLA and lignin were formulated specifically for FDM 3D printing. The results of the DSC analysis indicated that the incorporation of lignin led to a decrease in the glass transition temperature of PLA, from 71°C to 59°C. This reduction can be attributed to the enhanced intermolecular spacing and the introduction of stiff phenyl groups within the composite structure [33].

Thermogravimetric analysis (TGA) is a technique utilised to quantify the mass of a given sample in relation to both time and temperature. The primary purpose of its utilisation is to evaluate the thermal stability of a certain material. In their study, Wang et al. successfully fabricated nanocomposites for 3D printing by incorporating L-arg, graphite nanoplatelets, and polylactic acid. The inclusion of these materials resulted in a notable enhancement in thermal stability, as evidenced by a substantial increase of 60°C in the degradation temperature. This improvement in thermal stability not only expanded the processing window but also minimised the risk of thermal degradation occurring during the 3D printing procedure [38]. TGA is employed for the estimation of mineral content or deposition in the context of innovative material creation for 3D printing. In their study, Tanase-Opedal et al. conducted TGA on composites of PLA and lignin. They specifically focused on determining the residual mass of lignin when subjected to a temperature of 800°C. This temperature was chosen because lignin exhibited the formation of char, characterised by the presence of highly condensed aromatic structures, which enabled its retention at elevated temperatures [33].

3.7 OTHER APPLICATION-SPECIFIC TESTS

The utilisation of 3D printing technology has found widespread applications. Consequently, in addition to the conventional characterisation methods outlined earlier, it is imperative to take into account other characterisation methods that are relevant to the unique applications.

The utilisation of 3D printing technology has been implemented in the domain of microfluidics, including applications such as lab-on-a-chip systems and micro-thermal management, among others. The utilisation of 3D printing technology has facilitated the development of microfluidic connectors for microfluidic devices. The primary attribute of the 3D-printed connector is its dimensional correctness, as it has a direct impact on the fluid flow pathway. A further noteworthy characteristic of the 3D-printed fluid connector pertains to its maximum working pressure, denoting the highest level of pressure that the 3D-printed component can endure without experiencing any leakage. Pressure tests can be conducted using either liquid, typically water, or gas, typically compressed air or dry nitrogen. The pressure decreases inside the system or the development of bubbles upon submerging the objects in water serve as indicators of potential leaks (Figure 3.4) [39].

The utilisation of 3D printing technology for fabricating shape memory hydrogels has found significant applications within the domains of soft robotics, biomedicine, and sensing industries. The researchers Shiblee et al. created innovative hydrogels

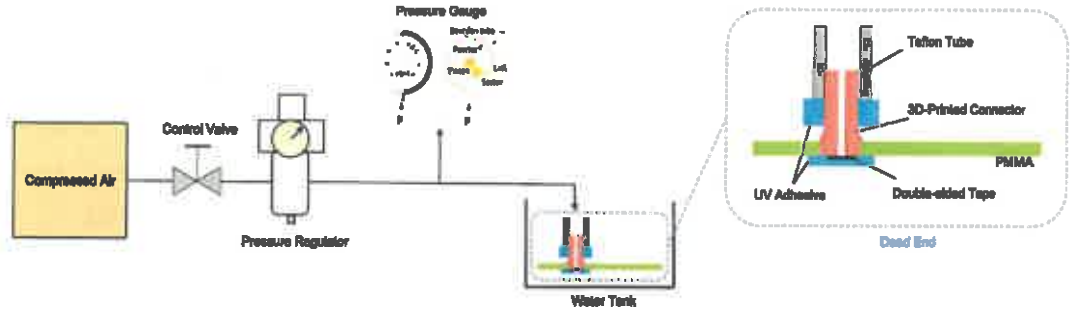

FIGURE 3.4 Pressure test of a 3D-printed connector for a microfluid device. Adapted from [39]. Copyright the authors, some rights reserved; exclusive licensee MDPI. Distributed under a Creative Commons Attribution License 4.0 (CC BY).

with shape memory properties specifically designed for use in SLA 3D printing. In addition to the conventional assessment of physiochemical, thermal, and mechanical properties, the shape memory property was rigorously assessed through the utilisation of a dynamic mechanical analyser employing a programmed thermomechanical technique. The samples were subjected to thermal equilibration at a temperature of 70°C for a duration of 10 minutes. Following this, a tensile load of 120 mN was applied to the samples. Subsequently, the samples were cooled to a temperature of –20°C, and the load was removed. The samples were then warmed to 70°C, and the recovery of the samples was observed [40].

The utilisation of 3D printing technology has been employed in the advancement of battery development. The researchers McOwen et al. successfully formulated 3D printing inks and used them to fabricate solid electrolytes for solid-state batteries. These solid electrolytes exhibited significantly reduced resistance in whole cell configurations, along with enhanced energy and power density. The process of material characterisation involved the use of various analytical techniques. XRD was employed to investigate the structure of the material, while a laser diffraction particle size distribution analyser was utilised to measure the particle size. Additionally, a rheometer was employed to determine the viscosity of the material, and SEM was utilised to examine the morphology of the material. Battery-related characterisation techniques were employed in this study. These techniques included the use of a potentiostat for conducting cell electroanalytical experiments, electrochemical impedance spectroscopy (EIS) for evaluating the ionic conductivity and interfacial charge transport of the developed material, and contact angle measurement for assessing the structural properties of the electrolyte–electrode interface [41, 42].

The utilisation of 3D printing technology presents numerous potential advantages to the field of biomedical science and industry. For example, the utilisation of 3D printing technology enables the production of porous scaffolds that possess meticulously regulated pore diameters, hence facilitating their application in the field of tissue engineering. Porous structures facilitate efficient mass transfer, hence influencing several biological processes such as cell migration, nutrition transportation, blood vessel infiltration, and tissue growth routes within the scaffold. Typically, conventional techniques are employed to characterise 3D-printed materials, including physiochemical analysis, porosity assessment, morphological examination, surface

roughness evaluation, mechanical testing, and other related methodologies. Various specific studies are conducted to evaluate the suitability of 3D-printed scaffolds for tissue engineering purposes. These tests include assessments of hydrophilicity as well as in vivo and in vitro biological testing [43].

The measurement of hydrophilicity can be quantified by the use of a goniometer, an instrument specifically designed for determining water contact angles. The experimental procedure involves the application of a small quantity of de-ionised pure water onto the test sample's surface, resulting in the formation of a liquid droplet. Subsequently, the angle formed between the fluid and the surface is determined and referred to as the contact angle. When the angle measures less than 90°, the test material is classified as hydrophilic. Conversely, when the angle measures larger than 90°, the test material is classified as hydrophobic. In their study, Vaidya et al. conducted research on the development of polyhydroxybutyrate (PHB) composites with lignin for the purpose of FDM 3D printing. The authors observed that as the lignin content in the composites grew, the contact angle also increased. This finding suggests that the inclusion of lignin in the composites leads to enhanced hydrophobic properties [44].

The in vitro characterisation of 3D-printed objects for medical applications typically involves the utilisation of cells derived from several sources, including people, rabbits, rats, pigs, goats, and bovines. The objective of the in vitro experiments is to evaluate the biocompatibility and osteogenic capacity of the test specimen. The evaluation of in vitro cell biocompatibility include the examination of cell attachment, cell viability, and cell proliferation. Cell attachment refers to the phenomenon of adhesion between cells and a surface. This biological process includes various molecular interactions, such as ligand binding and intracellular signalling. Cell adhesion plays a pivotal role in facilitating cellular cohesion both among cells themselves and with their surrounding environment. This fundamental process is of utmost importance in preserving the integrity and functionality of tissues. The incorporation of minerals into the polymer matrix has been shown to enhance cell adhesion [45]. Cell viability refers to the quantification of living cells within a given population, while cell proliferation pertains to the assessment of cell division. The assessment of cell viability and proliferation serves as a reliable approach to determine whether the test substance exhibits the capacity to stimulate cellular growth. In their study, Chen et al. fabricated composites of PLA and halloysite nanotubes for the purpose of coronary stent application. The investigation involved assessing the vitality and proliferation of human umbilical vein endothelial cells, which demonstrated that the composites exhibited biocompatibility and were deemed suitable for utilisation in this specific application [46].

The authors Kim et al. formulated a bioink by modifying silk fibroin with glycidyl methacrylate for the purpose of digital light 3D printing. To evaluate the compatibility of the bioink with living cells, specifically NIH/3T3 fibroblasts, a live/dead experiment was employed. The cells were suspended within the bioink that was formulated and subsequently printed using a digital light 3D printer. Following the printing process, the cells were then cultured for a period of 14 days. The cells that were enclosed within the bioink exhibited a predominantly viable state. The long-term biocompatibility of the bioink that was created was evaluated by the utilisation of a digital light 3D printing process to produce a ring-shaped trachea composed of cartilaginous

tissue. A 4-week in vitro investigation of the printed trachea revealed a remarkable proliferation of chondrocytes and the development of cartilage tissue [30].

The process of in vivo characterisation involves conducting tests and analyses inside the physiological context of a living organism. In their study, Moncal et al. utilised FDM 3D printing to fabricate bone scaffolds comprising composites of polycaprolactone, poly (D, L-lactide-co-glycolide), and hydroxyapatite. These scaffolds were subsequently implanted into rat calvarial defects to assess their in vivo performance. The findings of this investigation revealed that the composite scaffolds exhibited a significant level of newly mineralised bone tissue formation and degradation after 8 weeks of implantation, as reported in their publication [47].

3.8 CONCLUSION

The utilisation of 3D printing, a technology that is undergoing rapid development, has become prevalent across various industries. The methods employed for characterising 3D-printed things bear resemblance to those employed for conventionally created objects. In addition to the conventional testing and application-specific characterisation methods outlined in this chapter, it is noteworthy to see a growing inclination towards the integration of characterisation methods with the 3D printing process, enabling real-time monitoring of the 3D printing process. The application of a synchrotron imaging system to the laser 3D printing process using metal powder enables the real-time observation of the melting process and subsequent solidification of the powder [48]. ThermoFisher Scientific integrated rheology and Raman spectroscopy into the FDM 3D printing process in order to concurrently observe the impact of extrusion on the crystallisation kinetics and crystal structures of the 3D-printed items [49]. As the use of 3D printing technology continues to expand within the broader manufacturing environment, there will be ongoing advancements and refinement of the associated characterisation approaches.

REFERENCES

[1] Statista Research Department, Global 3D printing industry market size, Statista, 2021.
[2] J. Kacmarcik, D. Spahic, K. Varda, E. Porca, N. Zaimovic-Uzunovic, An investigation of geometrical accuracy of desktop 3D printers using CMM, IOP Conf. Ser. Mater. Sci. Eng. 393 (2018) 12085.
[3] K. Sandhu, G. Singh, S. Singh, R. Kumar, C. Prakash, S. Ramakrishna, G. Królczyk, C.I. Pruncu, Surface characteristics of machined polystyrene with 3D printed thermoplastic tool, Materials. 13 (2020) 2729.
[4] R. Thalmann, F. Meli, A. Küng, State of the art of tactile micro coordinate metrology, Appl. Sci. 6 (2016) 150.
[5] Y. Li, Y. Zhao, Z. Wang, C. Fang, W. Sha, Precision measurement method of laser beams based on coordinate measuring machine, IEEE Access. 7 (2019) 112736–112741.
[6] C.H. Lin, Y.M. Lin, Y.L. Lai, S.Y. Lee, Mechanical properties, accuracy, and cytotoxicity of UV-polymerized 3D printing resins composed of Bis-EMA, UDMA, and TEGDMA, J. Prosthet. Dent. 123 (2020) 349–354.
[7] T. Fang, M.A. Jafari, I. Bakhadyrov, A. Safari, S. Danforth, N. Langrana, On-line defect detection in layered manufacturing using process signature, Proc. IEEE Int. Conf. Syst. Man Cybern. 5 (1998) 4373–4378.

[8] J. Straub, Initial work on the characterization of additive manufacturing (3D printing) using software image analysis, Machines. 3 (2015) 55–71.
[9] E. Gkartzou, E.P. Koumoulos, C.A. Charitidis, Production and 3D printing processing of bio-based thermoplastic filament, Manuf. Rev. 4 (2017) 1.
[10] D.A. Lange, H.M. Jennings, S.P. Shah, Analysis of surface roughness using confocal microscopy, J. Mater. Sci. 28 (1993) 3879–3884.
[11] C. Polzin, S. Spath, H. Seitz, Characterization and evaluation of a PMMA-based 3D printing process, Rapid Prototyp. J. 19 (2013) 37–43.
[12] N.E. Gorji, R. O'Connor, D. Brabazon, X-ray tomography, AFM and Nanoindentation measurements for recyclability analysis of 316L powders in 3D printing process, Procedia Manuf. 47 (2020) 1113–1116.
[13] Z. Wang, L. Fuh, Effect of porosity on mechanical properties of 3D printed polymers: Experiments and micromechanical modeling based on X-ray computed tomography analysis, Polymers (Basel). 11 (2019) 1154.
[14] S. Yu, M. Xia, J. Sanjayan, L. Yang, J. Xiao, H. Du, Microstructural characterization of 3D printed concrete, J. Build. Eng. 44 (2021) 102948.
[15] H. Liu, K. Gong, A. Portela, Z. Cao, R. Dunbar, Y. Chen, Granule-based material extrusion is comparable to filament-base d material extrusion in terms of mechanical performances of printed PLA parts: A comprehensive investigation, Addit. Manuf. 75 (2023) 103744.
[16] N.A. Nguyen, S.H. Barnes, C.C. Bowland, K.M. Meek, K.C. Littrell, J.K. Keum, A.K. Naskar, A path for lignin valorization via additive manufacturing of high-performance sustainable composites with enhanced 3D printability, Sci. Adv. 4 (2018).
[17] J.R.C. Dizon, A.H. Espera, Q. Chen, R.C. Advincula, Mechanical characterization of 3D-printed polymers, Addit. Manuf. 20 (2018) 44–67.
[18] S.H. Ahn, M. Montero, D. Odell, S. Roundy, P.K. Wright, Anisotropic material properties of fused deposition modeling ABS, Rapid Prototyp. J. 8 (2002) 248–257.
[19] K. Korniejenko, M. Łach, S.Y. Chou, W.T. Lin, A. Cheng, M. Hebdowska-Krupa, S. Gadek, J. Mikuła, Mechanical properties of short fiber-reinforced geopolymers made by casted and 3D printing methods: A comparative study, Materials. 13 (2020) 579.
[20] J. Justo, L. Távara, L. García-Guzmán, F. París, Characterization of 3D printed long fibre reinforced composites, Compos. Struct. 185 (2018) 537–548.
[21] F. Mashayekhi, J. Bardon, V. Berthe, H. Perrin, S. Westermann, F. Addiego, Fused filament fabrication for polymers and continuous fiber-reinforced polymer composites: Advance in structure optimization and health monitoring, Polymers (Basel). 13 (2021).
[22] P. Parandoush, D. Lin, A review on additive manufacturing of polymer-fiber composites, Compos. Struct. 182 (2017) 36–53.
[23] M.R. Khosravani, F. Berto, M.R. Ayatollahi, T. Reinicke, Characterization of 3D-printed PLA parts with different raster orientations and printing speeds, Sci. Rep. 121. 12 (2022) 1–9.
[24] B. Rankouhi, S. Javadpour, F. Delfanian, T. Letcher, Failure analysis and mechanical characterization of 3D printed ABS with respect to layer thickness and orientation, J. Fail. Anal. Prev. 16 (2016) 467–481.
[25] Z. Zguris, How mechanical properties of stereolithography 3D prints are affected by UV curing, Formlabs White Pap. (2022). https://go.eacpds.com/acton/attachment/25728/f-069f/1/-/-/-/-/Formlabs%20How%20Mechanical%20Properties%20of%20SLA%203D%20Prints%20are%20affected%20by%20UV%20Curing.pdf
[26] S.U. Zhang, Degradation classification of 3D printing thermoplastics using fourier transform infrared spectroscopy and artificial neural networks, Appl. Sci. 8 (2018) 1224.
[27] F. Carrasco, P. Pagès, J. Gámez-Pérez, O.O. Santana, M.L. Maspoch, Processing of poly(lactic acid): Characterization of chemical structure, thermal stability and mechanical properties, Polym. Degrad. Stab. 95 (2010) 116–125.

[28] J. Roman, W. Neri, V. Fierro, A. Celzard, A. Bentaleb, I. Ly, J. Zhong, A. Derré, P. Poulin, Lignin-graphene oxide inks for 3D printing of graphitic materials with tunable density, Nano Today. 33 (2020) 100881.
[29] S.J. Trenfield, P. Januskaite, A. Goyanes, D. Wilsdon, M. Rowland, S. Gaisford, A.W. Basit, Prediction of solid-state form of SLS 3D printed medicines using NIR and Raman spectroscopy, Pharm. 14 (2022) 589.
[30] S.H. Kim, Y.K. Yeon, J.M. Lee, J.R. Chao, Y.J. Lee, Y.B. Seo, M.T. Sultan, O.J. Lee, J.S. Lee, S. Il Yoon, I.S. Hong, G. Khang, S.J. Lee, J.J. Yoo, C.H. Park, Precisely printable and biocompatible silk fibroin bioink for digital light processing 3D printing, Nat. Commun. 91. 9 (2018) 1–14.
[31] P.D. Desai, R.N. Jagtap, Synthesis and characterization of fiber-reinforced resorcinol epoxy acrylate applied to stereolithography 3D printing, ACS Omega. 6 (2021) 31122–31131.
[32] J. Domínguez-Robles, N.K. Martin, M.L. Fong, S.A. Stewart, N.J. Irwin, M.I. Rial-Hermida, R.F. Donnelly, E. Larrañeta, Antioxidant PLA composites containing lignin for 3D printing applications: A potential material for healthcare applications, Pharmaceutics. 11 (2019).
[33] M. Tanase-Opedal, E. Espinosa, A. Rodríguez, G. Chinga-Carrasco, Lignin: A biopolymer from forestry biomass for biocomposites and 3D printing, Materials. 12 (2019) 3006.
[34] Z. Hu, F. Chen, J. Xu, Q. Nian, D. Lin, C. Chen, X. Zhu, Y. Chen, M. Zhang, 3D printing graphene-aluminum nanocomposites, J. Alloys Compd. 746 (2018) 269–276.
[35] L. Wang, W. Gao, S. Ng, M. Pumera, Chiral protein-covalent organic framework 3D-printed structures as chiral biosensors, Anal. Chem. 93 (2021) 5277–5283.
[36] Q. Zhang, M. Pardo, Y. Rudich, I. Kaplan-Ashiri, J.P.S. Wong, A.Y. Davis, M.S. Black, R.J. Weber, Chemical composition and toxicity of particles emitted from a consumer-level 3D printer using various materials, Environ. Sci. Technol. 53 (2019) 12054–12061.
[37] B. Damadzadeh, H. Jabari, M. Skrifvars, K. Airola, N. Moritz, P.K. Vallittu, Effect of ceramic filler content on the mechanical and thermal behaviour of poly-l-lactic acid and poly-l-lactic-co-glycolic acid composites for medical applications, J. Mater. Sci. Mater. Med. 21 (2010) 2523–2531.
[38] Y. Wang, M. Lei, Q. Wei, Y. Wang, J. Zhang, Y. Guo, J. Saroia, 3D printing biocompatible l-Arg/GNPs/PLA nanocomposites with enhanced mechanical property and thermal stability, J. Mater. Sci. 2020 5512. 55 (2020) 5064–5078.
[39] Q. Xu, J.C.C. Lo, S.R. Lee, Characterization and evaluation of 3D-printed connectors for microfluidics characterization and evaluation of 3D-printed connectors for, Micromachines. 12 (2021) 874.
[40] M.D.N.I. Shiblee, K. Ahmed, A. Khosla, M. Kawakami, H. Furukawa, 3D printing of shape memory hydrogels with tunable mechanical properties, Soft Matter. 14 (2018) 7809–7817.
[41] D.W. McOwen, S. Xu, Y. Gong, Y. Wen, G.L. Godbey, J.E. Gritton, T.R. Hamann, J. Dai, G.T. Hitz, L. Hu, E.D. Wachsman, 3D-printing electrolytes for solid-state batteries, Adv. Mater. 30 (2018).
[42] C. Wang, K. Fu, S.P. Kammampata, D.W. McOwen, A.J. Samson, L. Zhang, G.T. Hitz, A.M. Nolan, E.D. Wachsman, Y. Mo, V. Thangadurai, L. Hu, Garnet-type solid-state electrolytes: Materials, interfaces, and batteries, Chem. Rev. 120 (2020) 4257–4300.
[43] C.N. Kelly, A.T. Miller, S.J. Hollister, R.E. Guldberg, K. Gall, Design and structure–function characterization of 3D printed synthetic porous biomaterials for tissue engineering, Adv. Healthc. Mater. 7 (2018) 1–16.
[44] A.A. Vaidya, C. Collet, M. Gaugler, G. Lloyd-Jones, Integrating softwood biorefinery lignin into polyhydroxybutyrate composites and application in 3D printing, Mater. Today Commun. 19 (2019) 286–296.
[45] J. Huang, J. Xiong, J. Liu, W. Zhu, J. Chen, L. Duan, J. Zhang, D. Wang, Evaluation of the novel three-dimensional porous poly (L-lactic acid)/nanohydroxyapatite composite scaffold, Biomed. Mater. Eng. 26 (2015) S197–S205.

[46] Y. Chen, A. Murphy, D. Scholz, L.M. Geever, J.G. Lyons, D.M. Devine, Surface-modified halloysite nanotubes reinforced poly(lactic acid) for use in biodegradable coronary stents, J. Appl. Polym. Sci. 135 (2018) 46521.

[47] K.K. Moncal, D.N. Heo, K.P. Godzik, D.M. Sosnoski, O.D. Mrowczynski, E. Rizk, V. Ozbolat, S.M. Tucker, E.M. Gerhard, M. Dey, G.S. Lewis, J. Yang, I.T. Ozbolat, 3D printing of poly(ε-caprolactone)/poly(D,L-lactide-co-glycolide)/hydroxyapatite composite constructs for bone tissue engineering, J. Mater. Res. 33 (2018) 1972–1986.

[48] C.L.A. Leung, S. Marussi, R.C. Atwood, M. Towrie, P.J. Withers, P.D. Lee, In situ X-ray imaging of defect and molten pool dynamics in laser additive manufacturing, Nat. Commun. 2018 91. 9 (2018) 1–9.

[49] C.D. Millholland, Combining rheology and Raman spectroscopy to analyze 3D printing polymers—advancing materials, ThermoFisher Sci. (2019). https://www.thermofisher.com/blog/materials/combining-rheology-and-raman-spectroscopy-to-analyze-3d-printing-polymers/